Synthetic biology identifies the minimal gene set required for paclitaxel biosynthesis in a plant chassis

Youjun Zhang[1,2,*], Lorenz Wiese[3], Hao Fang[3,4], Saleh Alseekh[1,2], Leonardo Perez de Souza[1], Federico Scossa[1,5], John J. Molloy[4], Mathias Christmann[3] and Alisdair R. Fernie[1,2,*]

[1]Max-Planck-Institut für Molekulare Pflanzenphysiologie, Am Mühlenberg 1, 14476 Potsdam-Golm, Germany

[2]Center of Plant Systems Biology and Biotechnology, 4000 Plovdiv, Bulgaria

[3]Institute of Chemistry and Biochemistry, Freie Universität Berlin, Takustraße 3, 14195 Berlin, Germany

[4]Department of Biomolecular Systems, Max Planck Institute of Colloids and Interfaces, 14476 Potsdam, Germany

[5]Research Center for Genomics and Bioinformatics (CREA-GB), Via Ardeatina 546, 00178 Rome, Italy

*Correspondence: Youjun Zhang (yozhang@mpimp-golm.mpg.de), Alisdair R. Fernie (fernie@mpimp-golm.mpg.de)

https://doi.org/10.1016/j.molp.2023.10.016

ABSTRACT

The diterpenoid paclitaxel (Taxol) is a chemotherapy medication widely used as a first-line treatment against several types of solid cancers. The supply of paclitaxel from natural sources is limited. However, missing knowledge about the genes involved in several specific metabolic steps of paclitaxel biosynthesis has rendered it difficult to engineer the full pathway. In this study, we used a combination of transcriptomics, cell biology, metabolomics, and pathway reconstitution to identify the complete gene set required for the heterologous production of paclitaxel. We identified the missing steps from the current model of paclitaxel biosynthesis and confirmed the activity of most of the missing enzymes via heterologous expression in *Nicotiana benthamiana*. Notably, we identified a new C4β-C20 epoxidase that could overcome the first bottleneck of metabolic engineering. We used both previously characterized and newly identified oxomutases/epoxidases, taxane 1β-hydroxylase, taxane 9α-hydroxylase, taxane 9α-dioxygenase, and phenylalanine-CoA ligase, to successfully biosynthesize the key intermediate baccatin III and to convert baccatin III into paclitaxel in *N. benthamiana*. In combination, these approaches establish a metabolic route to taxoid biosynthesis and provide insights into the unique chemistry that plants use to generate complex bioactive metabolites.

Key words: paclitaxel biosynthesis, synthetic biology, baccatin III biosynthesis, *Taxus*

INTRODUCTION

As a major source of bioactive small molecules, medicinal plants represent important resources for treatments against several human diseases. Since the mid-1800s, the toxicity of Taxaceae extracts to animals has attracted the attention of chemists (Lucas, 1856). An unusual cyclic diterpenoid (paclitaxel) was isolated and characterized from the bark of the Pacific yew (*Taxus brevifolia*) (Wani et al., 1971) and was later shown to bind to β-tubulin, thereby destabilizing the assembly of microtubules. This activity of paclitaxel results in the slowing or blocking of mitosis at the metaphase-anaphase transition and ultimately causes the induction of apoptotic cell death (Yang and Horwitz, 2017). Since 1992, paclitaxel, under the brand name Taxol, has been approved by the US Food and Drug Administration for medical use against

several solid cancers (ovarian, breast, lung, cervical, pancreatic, and Kaposi's sarcoma) (Fischer and Ganellin, 2010). Subsequently, Taxol and some of its related taxane analogs (e.g., docetaxel) have become leading anti-cancer drugs, with sales reported to exceed five billion USD per year (Onrubia et al., 2013). Originally, paclitaxel was directly extracted from twigs, bark, or needles of pacific yew, but the low yield and the amount generally required for a therapeutic cycle (2–3 g paclitaxel/patient) have intensified the search for alternative approaches to produce paclitaxel (Li et al., 2019). Total chemical synthesis of paclitaxel, achieved for the first time in 1994, is not an economically
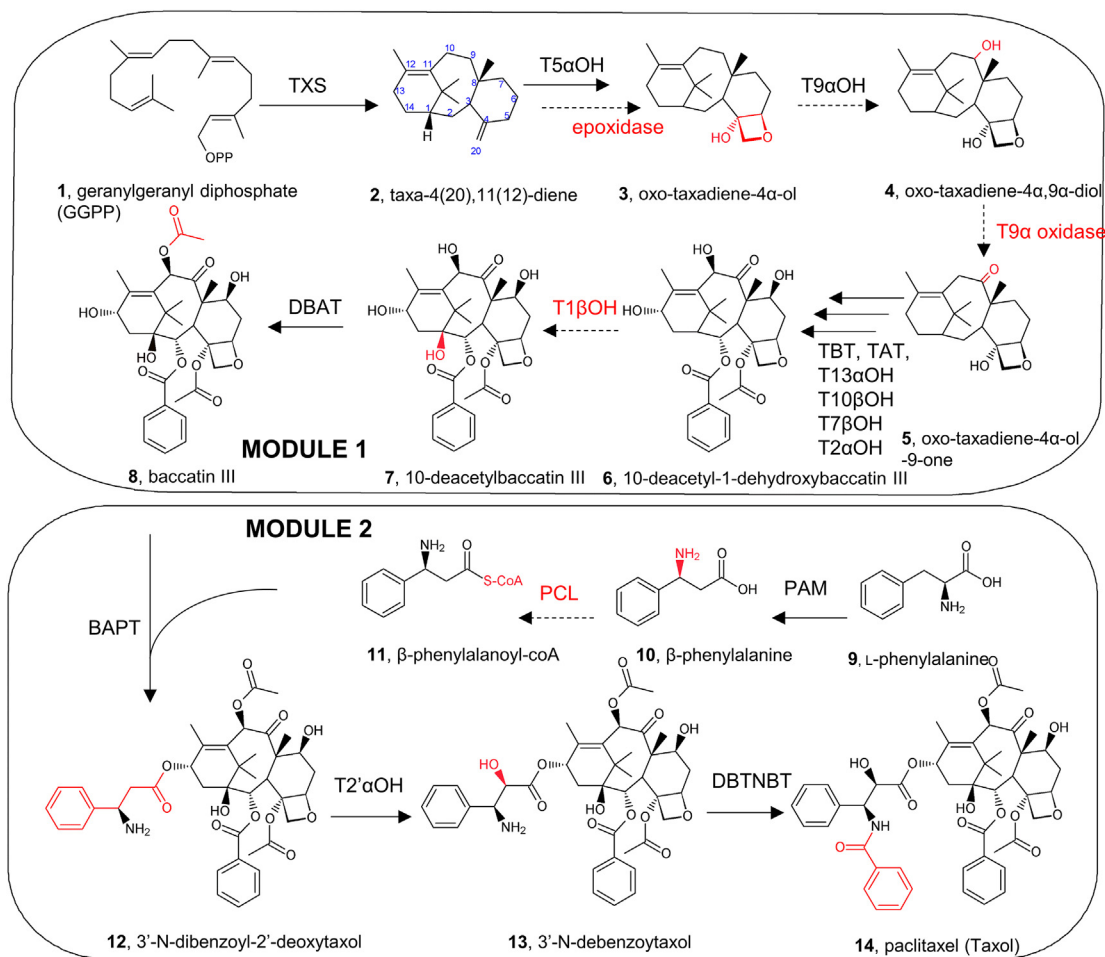

Figure 1. The pathway of paclitaxel biosynthesis.

The catalytic sequence of seven hydrogenation steps is unclear. The black dotted line and the red enzyme represent newly identified steps. A black color represents previously identified steps. Module 1 represents baccatin III biosynthesis. Module 2 represents the second part of the pathway. TXS, taxadiene synthase; T5αOH, taxane 5α-hydroxylase; TAT, taxadiene-5α-ol-O-acetyl transferase; T10βOH, taxane 10β-hydroxylase; T13αOH, taxane 13α-hydroxylase; T2αOH, taxane 2α-hydroxylase; T9αOH, taxane 9α-hydroxylase; T7βOH, taxane 7β-hydroxylase; T1βOH, taxane 1β-hydroxylase; TBT, taxane-2α-O-benzoyltransferase; DBAT, 10-deacetyl baccatin III-10-O-acetyltransferase; BAPT, baccatin III-3-amino, 13-phenylpropanoyltransferase; T2′αOH, taxane 2′α-hydroxylase; DBTNBT, 3′-N-debenzoyl-2′-deoxytaxol-N-benzoyltransferase; PAM, phenylalanine aminomutase; PCL, β-phenylalanine coenzyme A ligase.

sustainable alternative (Nicolaou et al., 1994). Paclitaxel production for medical use is currently based on a semi-synthetic approach, using 10-deacetylbaccatin III isolated from *Taxus* needles as a starting material for chemical synthesis. Plant cell cultures derived from several *Taxus* species are also employed for commercial paclitaxel production. Ideally, metabolic engineering approaches could be used to enhance paclitaxel levels in *Taxus* cell culture (Roberts, 2007; Nazhand et al., 2020; Mutanda et al., 2021) or to reconstitute paclitaxel production in a heterologous host such as *Saccharomyces cerevisiae* (Zhou et al., 2015). However, the biosynthetic pathway for paclitaxel must first be fully elucidated for metabolic engineering strategies to be feasible.

The biosynthesis of taxadiene (taxa-4(5),11(12)-diene,15), a C_{20} terpenoid, is the first committed step in the production of paclitaxel. Taxadiene is formed in the plastid by the action of taxadiene synthase (TXS) (Köksal et al., 2011), an enzyme using geranylgeranyl pyrophosphate produced through the methylerythritol phosphate pathway as substrate (De La Peña and Sattely, 2021). Taxadiene

is then presumably transported to the endoplasmic reticulum (ER), where it is further modified by at least 19 enzymes (Guerra-Bubb et al., 2012). In particular, taxadiene is hydroxylated at the C1, C2, C5, C7, C9, C10, and C13 positions, with further oxidation occurring at the C9 position (Guerra-Bubb et al., 2012; Zhang et al., 2021) (Figure 1). After further modifications, including acetylation and formation of the oxetane ring, the resulting intermediate, baccatin III (8), is subjected to the final decoration steps, which include the attachment of a β-phenylalanoyl moiety to C-13, additional oxidation of C-2α, and transfer of a benzoyl moiety on the same β-phenylalanoyl side chain (Figure 1). The enzymes responsible for 12 of these steps have been identified and well characterized (Onrubia et al., 2014; Ramírez-Estrada et al., 2016; Sanchez-Muñoz et al., 2020), but for at least six additional hypothetical reactions, presumably catalyzed by phenylalanine-CoA ligase (PCL), taxane 1β-hydroxylase (T1βOH), taxane 9α-hydroxylase (T9αOH), and taxane 9α-dioxygenase, molecular evidence is lacking, despite numerous omics resources that are now available for *Taxus*, including the recent release of the
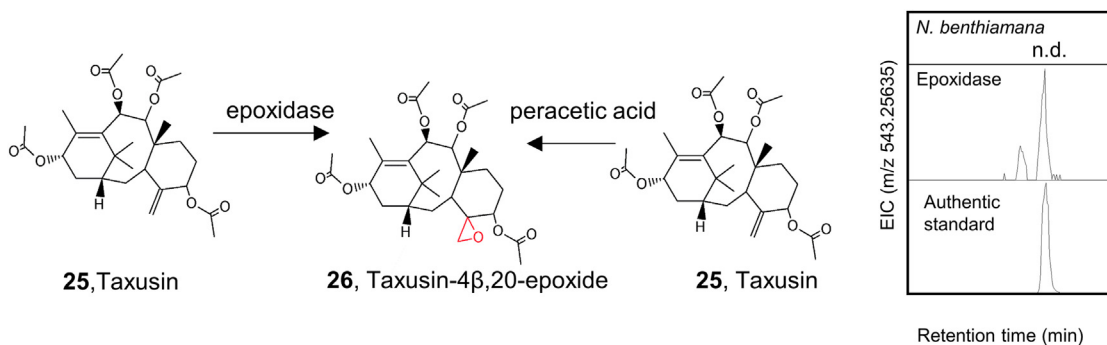
Figure 2. Identification of epoxidase.
Enzyme assay of epoxidase using taxusin as substrate. The generation of taxusin-4β,20-epoxide (26) by either enzyme assay or chemical synthesis was confirmed by NMR. n.d., not detected.

genome sequence of *Taxus chinensis* var. *mairei* (Cheng et al., 2021; Xiong et al., 2021; Zhang et al., 2021). Here, we report the discovery of these missing paclitaxel biosynthetic enzymes, verified by the reconstitution of the baccatin III and paclitaxel pathways in the heterologous host *N. benthamiana* (Figure 1).

RESULTS

Identification of candidate genes completing the pathway of paclitaxel biosynthesis

Genes of plant specialized biosynthetic pathways are often co-expressed (Mutwil, 2020). We utilized this characteristic to search for candidate genes for the missing steps of paclitaxel biosynthesis across multiple published RNA sequencing (RNA-seq) datasets using the 12 previously characterized paclitaxel biosynthesis genes as bait (Ramírez-Estrada et al., 2016; Liao et al., 2017; Kuang et al., 2019; Zhou et al., 2019) (Supplemental Figure 1). Expression of the 12 characterized paclitaxel biosynthesis genes could be detected in these RNA-seq datasets, and a further 37 uncharacterized potential biosynthetic gene candidates were found to be co-expressed with these known genes (Supplemental Table 1). Moreover, three chemicals (10-deacetylbaccatin III, baccatin III and paclitaxel) could not be detected in *N. benthamiana*, which indicated that this species could be used to verify the function of these genes (Supplemental Figures 2 and 3). Given the high complexity of paclitaxel biosynthesis, we split the pathway into two modules: (i) 10-deacetylbaccatin III and baccatin III biosynthesis and (ii) the late stages of paclitaxel production from baccatin III (Figure 1).

Epoxidation reactions of baccatin III biosynthesis

The biosynthetic genes for the biosynthetic intermediate taxadiene have been successfully transferred to *E. coli* (Ajikumar et al., 2010), yeast (Zhou et al., 2015), and tobacco chloroplasts (Li et al., 2019; De La Peña and Sattely, 2021). However, how the pathway proceeds immediately downstream is less clear. It is proposed that the CYP725A4 taxane-5α-hydroxylase (T5αOH) converts taxadiene into taxadiene-5α-ol (16), but enzyme assays show that T5αOH produces primarily 5(12)-oxa-3 (11)-cyclotaxane (OCT; 17), which can no longer re-enter the route to paclitaxel (Zhou et al., 2015; Edgar et al., 2017; Li et al., 2019; Mutanda et al., 2021) (Supplemental Figures 4–8).

Subsequently, we optimized production of taxadiene in *N. benthamiana* using previously reported approaches. We transiently expressed truncated versions of the diterpene synthase TXS (nsTXS) and geranylgeranyl pyrophosphate synthase (nsGGPS) that were targeted to the cytosol instead of the plastid, along with the rate-limiting enzyme of the cytosolic mevalonate-dependent isoprenoid pathway, 3-hydroxy-3-methylglutaryl-CoA reductase (HMGR) (Rontein et al., 2008; Li et al., 2019; De La Peña and Sattely, 2021). Approximately 100 μg taxadiene per gram fresh weight (FW) of *N. benthamiana* leaf was obtained.

With an optimized taxadiene production platform in hand, we set about screening the biosynthetic gene candidates that encoded oxidases to see if one of these candidates could use taxadiene as a substrate. When one of the candidates, encoding a 2-oxoglutarate/Fe(II)-dependent dioxygenase (epoxidase) (Ramírez-Estrada et al., 2016), was expressed in *N. benthamina* along with nsTXS1, nsGGPS, and HMGR, we observed three ion peaks related to a compound with *m/z* 288 following derivatization-based gas chromatography–mass spectrometry (GC–MS) analysis of an ethyl acetate extract of the *N. benthamiana* leaf tissue (Supplemental Figures 9 and 10). None of these spectra matched OCT (17), iso-OCT (18), taxadiene-5α-ol (16), or chemically synthesized epoxide-taxadiene (Supplemental Figures 5 and 10). We attempted to express this putative 4β-C20 epoxidase (19) in *E. coli* or *S. cerevisiae* strains that produced taxadiene. However, in both instances, only the taxadiene starting material could be detected, suggesting that this enzyme cannot be expressed in active form in these expression systems. However, when we transiently expressed T5αOH, along with HMGR, nsGGPS, nsTXS, and epoxidase, the level of oxidized taxadiene was significantly reduced, suggesting that it is a substrate of the downstream enzymes of the paclitaxel pathway (Supplemental Figures 9–14).

Moreover, using the synthesized taxusin-4β,20-epoxide (26) as an authentic standard (Kaspera et al., 2010), we were able to demonstrate that the epoxidase could catalyze the conversion of taxusin (25) to taxusin-4β,20-epoxide (26, high-resolution MS [HRMS] *m/z* 543.25572 [M⁺+Na]) (Figure 2; Supplemental Figures 15 and 16). This suggests that the epoxidase may catalyze an epoxidation of C4-20, but since we were unable to isolate any of the epoxidase products in quantities sufficient for nuclear magnetic resonance (NMR), the catalytic activity of this
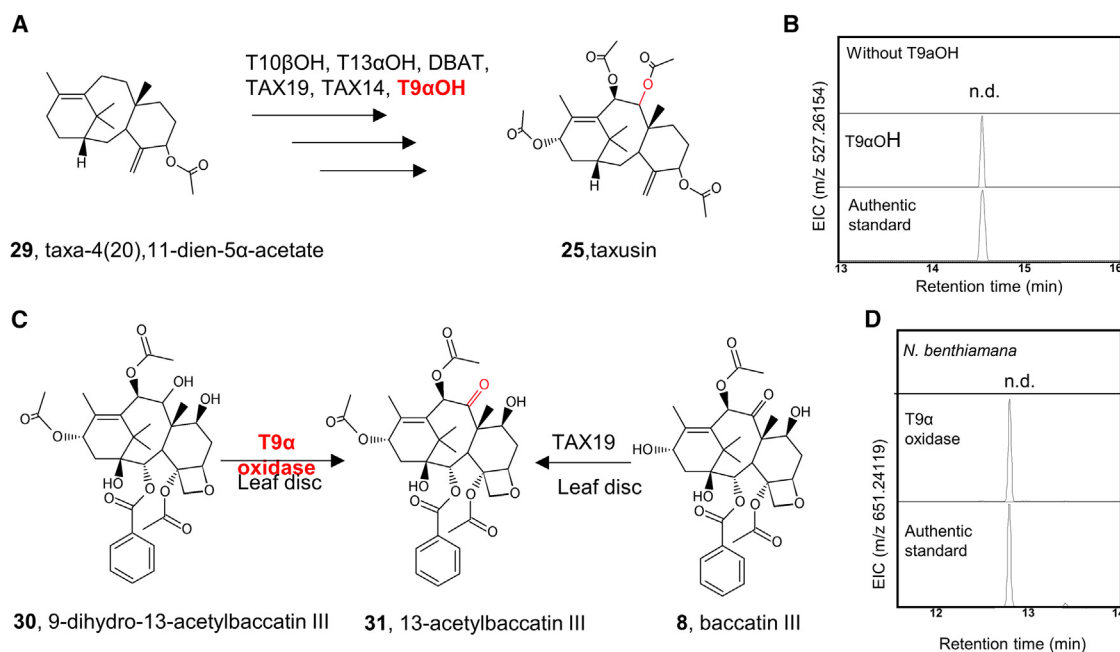
Figure 3. Identification of T9αOH and T9α oxidase.
(A) Biosynthesis of taxusin from taxa-4(20),11-dien-5α-acetate (29) with newly identified T9αOH alongside T10βOH, T13αOH, DBAT, TAX19, and TAX14.
(B) LC–MS confirmation of the products of taxusin with and without T9αOH compared with the authentic standard of taxusin.
(C) 13-Acetylbaccatin III (31) could be generated by either T9α oxidase or TAX19. TAX19 is the taxoid-O-acetyltransferase acting at the C13 position to generate 13-acetylbaccatin III (31).
(D) LC–MS analysis of 13-acetylbaccatin III(31) produced from the two different enzymes and substrates and compared with the authentic standard (confirmed by NMR).

epoxidase remains speculative, and future research will be needed in order to unambiguously define this stage of the pathway.

Identification of two missing hydroxylases

The enzyme in the next missing step is predicted to be a taxoid 9α-hydroxylase. Based on the transcriptomic analysis, 12 new cytochrome P450s were found with high sequence similarity to the other five taxadiene hydroxylation enzymes, including three potential T9αOHs. Thus, we screened all potential proteins to determine if they were capable of acting as distinct hydroxylases by expressing the selected enzymes alongside nsTXS1, nsGGPS, 4β-C20 epoxidase, HMGR, and RNA silencing suppressor p19 in *N. benthamiana* leaves (Supplemental Figure 17). The expression CYP725A22-1 was found to significantly reduce the levels of the 4β-C20 epoxidase (19) and to produce novel metabolic intermediates with *m/z* 304 in GC-MS, a mass consistent with C5 or C10 hydroxylation (Supplemental Figure 17). This peak has mass spectral profiles and a retention time distinct from those of products generated by all five characterized hydroxylases. To confirm this taxoid 9α-hydroxylase, we synthesized taxusin (25) using previously characterized enzymes (T10βOH, taxane 13α-hydroxylase, 10-deacetyl baccatin III-10-O-acetyltransferase [DBAT], TAX19, TAX14) alongside the newly identified T9αOH (Figure 3A) by supplying taxa-4(20),11-dien-5α-acetate (29). As assessed by the production of taxusin (25), which we followed by liquid chromatography–tandem MS (LC–MS/MS), the presence of T9αOH could overcome the limitation of using taxadiene-5α,13α-ol (32) or taxadiene-5α-yl-acetate-10β-diol (33) as a precursor, which was stated in previous publications (Jennewein et al., 2001; Guerra-Bubb et al., 2012) (Supplemental Figure 18).

Given that both taxane 7β-hydroxylase and taxane 2α-hydroxylase were found to display activity using taxusin (25) as substrate (Chau et al., 2004a), we independently expressed 12 new cytochrome P450s iin *N. benthamiana* leaves, which were subsequently fed with taxusin (25). Hydroxylased taxusin, which has a distinct retention time but the same spectral profile as 7β-hydroxytaxusin (36) and 2α-hydroxytaxusin (37), was generated by CYP725A23-1 (Supplemental Figure 19). To confirm the function of the 4β-C20 epoxidase, T9α oxidase, T9αOH, and taxane 1β-hydroxylase candidates within the paclitaxel pathway, all the identified enzymes of baccatin III (8) biosynthesis (i.e., the 12 known enzymes plus these four novel enzymes) were expressed in *N. benthamiana* leaves as described below.

Discovery of the missing T9α oxidase

An oxidase that acts on carbon 9 (T9 α oxidase) is anticipated to be essential for the formation of baccatin III (8), but the responsible protein has not yet been identified. Supplying 9-dihydro-13-acetylbaccatin III (30) to tobacco leaves expressing one of the gene candidates, which was homologous to gibberellin 20-oxidase (2-oxoglutarate/Fe(II)-dependent dioxygenase), resulted in the production of 13-acetylbaccatin III (31) by C9 oxidation (Figure 3; Supplemental Figures 20 and 21). The 13-acetylbaccatin III (31) could also be generated from baccatin III (8) by C13 acetylation (Chau et al., 2004b). Similarly, supplying *N. benthamiana* expressing taxane-2α-O-benzoyltransferase, DBAT, T9 α oxidase, and taxadiene-5α-ol-O-acetyl transferase with deacetyl-9-dihydro-13-acetylbaccatin III (39) as an exogenously supplied substrate resulted in the production of baccatin III (8) (Supplemental Figure 22). A mechanism for spontaneous
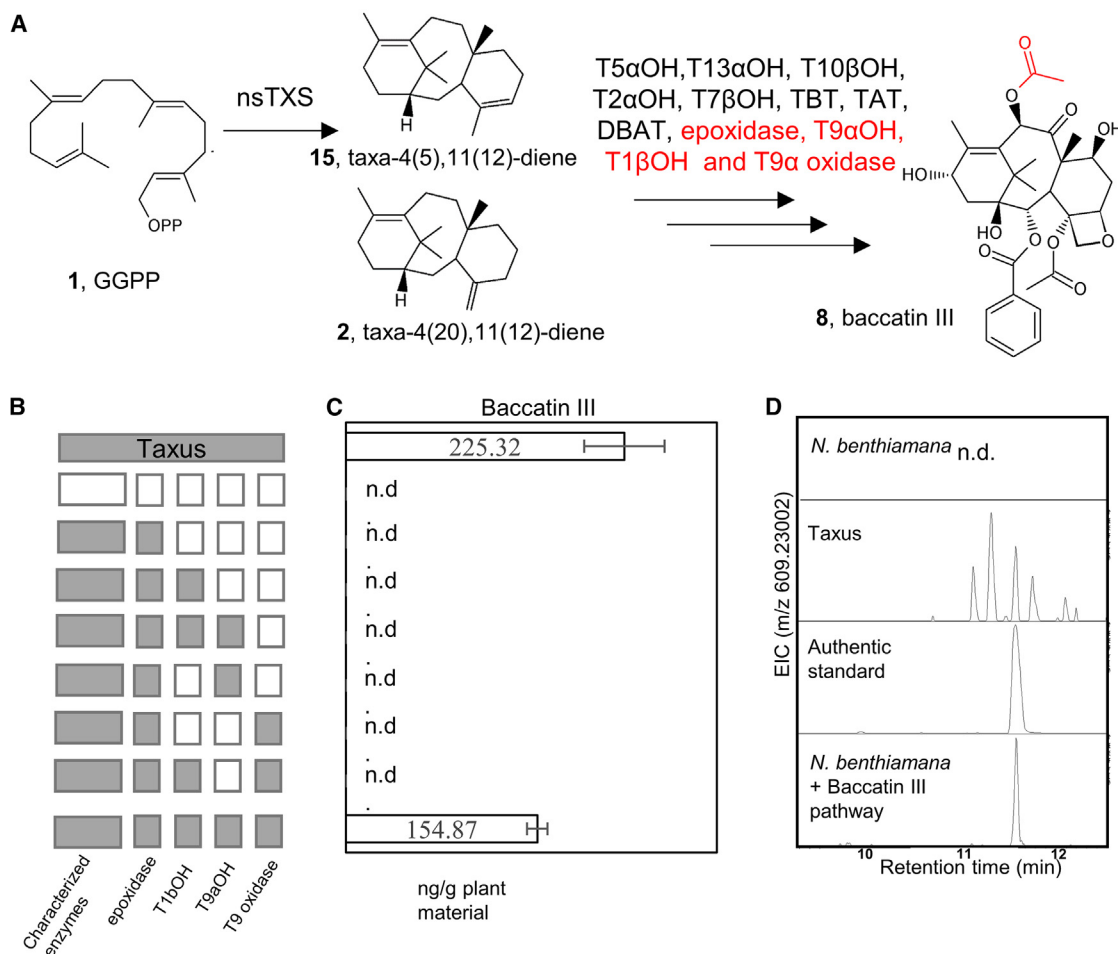
Figure 4. Biosynthesis of baccatin III(8) in *N. benthamiana*.
(A) Scheme of baccatin III(8) biosynthesis.
(B) The characterized enzymes (T5αOH, T13αOH, T10βOH, T2αOH, T7βOH, TBT, TAT, DBAT) were expressed with four newly identified enzymes to produce baccatin III (8).
(C) Around 154.87 ng/g baccatin III (8) was produced from four biological replicates compared with 225.32 ng/g in *Taxus* needles.
(D) The identification of baccatin III (8) from taxus, authentic standard, and infiltrated *N. benthamiana*. Error bars represent standard deviation. n.d., not detected.

formation of the oxetane ring has been suggested in previous research (Ondari and Walker, 2008; Guerra-Bubb et al., 2012) (Supplemental Figure 23). Here, the spontaneous transfer of the deacetyl-1-hydroxybaccatin I (43) oxetane ring to deacetyl-9-dihydro-13-acetylbaccatin III (39) was also observed (Supplemental Figure 24). Moreover, deacetylated taxusin (44) could not be used for baccatin III biosynthesis in our feeding experiment, the same finding as in previous research (Supplemental Figure 25) (Ondari and Walker, 2008; Guerra-Bubb et al., 2012).

Engineering baccatin III biosynthesis

The use of heterologous hosts for paclitaxel production represents a research priority, given the complexity and associated costs of the current alternative approach based on semi-synthesis. In this regard, *Arabidopsis* and *Nicotiana* are expected to offer a favorable environment for the functional expression of CYP450s and the other genes involved in the biosynthesis of paclitaxel pathway intermediates. The two main bottlenecks hindering the elucidation of the full Taxol pathway are the lack of detection of many putative intermediates and the insufficient data concerning the localization and the transport of these intermediates at the subcellular level. Thus, we engineered all baccatin III (8) biosynthetic genes, including *P19*, *3-hydroxy-3-methylglutaryl coenzyme A reductase* (*HMGR*), and *benzoate-Coenzyme A ligase* (*BZL*), so that their products were located in either the cytosol or at the ER membrane. The engineered DBAT, which has been demonstrated to possess superior catalytic properties (estimated to be 60 times more efficient than DBAT) (You et al., 2018), was also used. Although the co-transformation efficiency of these three large plasmids remained low, we found that both 10-deacetylbaccatin III (7) and baccatin III (8) were produced in all replications in *N. benthamiana* leaves (Figure 4A; Supplemental Figures 26–28). Although the level of 10-deacetylbaccatin III (7) was relatively low (~15.40 ng/g FW), the levels of baccatin III (8) could reach ~154.84 ng/g FW in *N. benthamiana*, which is close to the amount produced in *Taxus* needles (~225.32 ng/g FW). Despite the lower yield than that found when the genes are expressed in their native environment, these
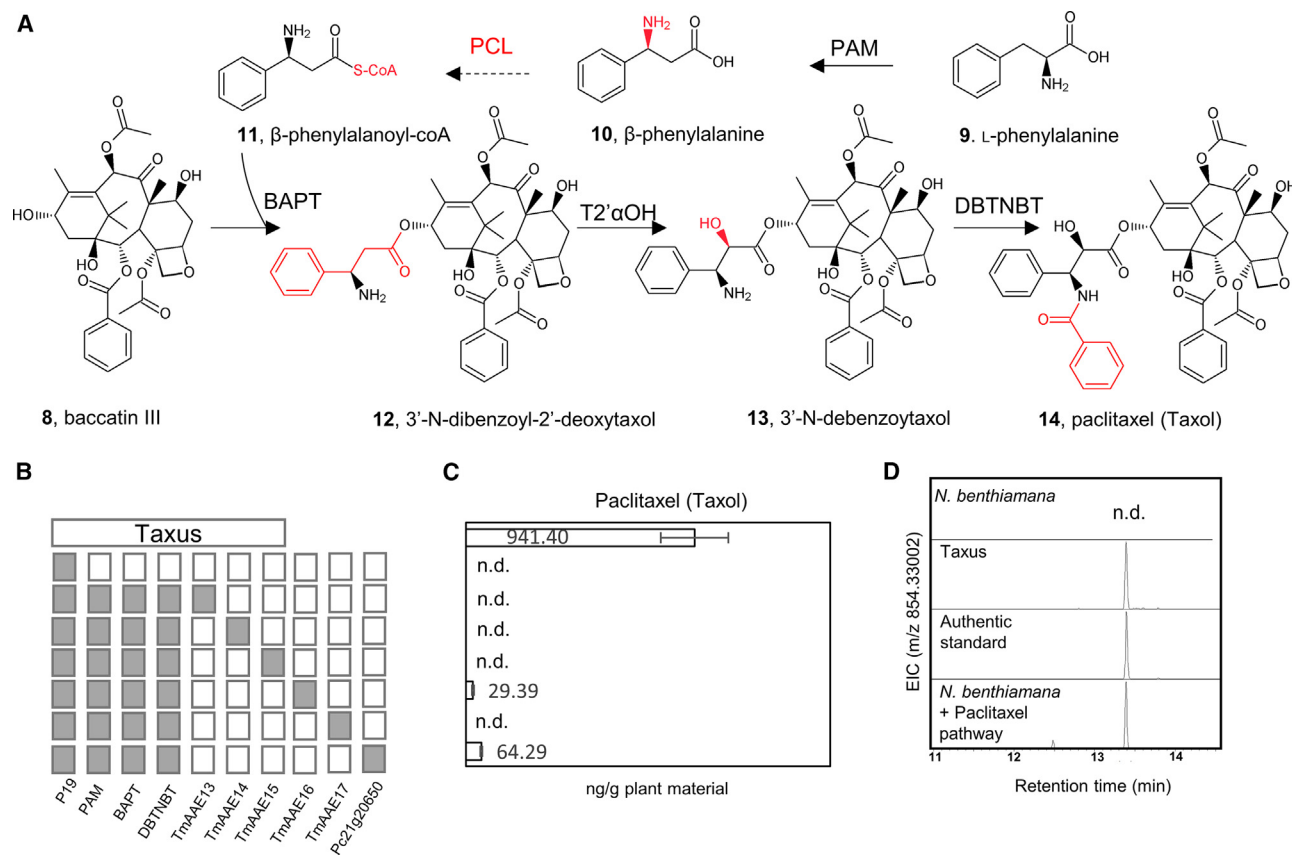
Figure 5. Identification of the missing PCL and confirmation of the activity of T2′αOH.

(A) Scheme of paclitaxel(14) biosynthesis from baccatin III(8) and L-phenylalanine(9).

(B) Expression of the three characterized enzymes (PAM, BAPT, and DBTNBT) with the newly identified enzymes to produce paclitaxel by feeding baccatin III(8) and L-pheylalanine(9).

(C) Paclitaxel(14) was produced by TmAAE16 (∼29.39 ng/g) and Pc21g20650 (∼64.29 ng/g) in *N. benthamiana*. *Taxus* needles produced around 941.40 ng/g paclitaxel.

(D) The identification of paclitaxel(14) from taxus, authentic standard, and infiltrated *N. benthamiana.* Error bars represent standard deviation. n.d., not detected.

results showed that we can produce 10-deacetylbaccatin III (7) and baccatin III (8) in a heterologous system, having defined an entire minimal pathway for their biosynthesis (Figure 4; Supplemental Figures 26 and 29). As a final experiment regarding the pathway structure, we carried out a so-called dropout experiment in which the entire pathway of baccatin III (8) biosynthesis was expressed in *N. benthamiana* leaves with the exception of one gene at a time. Without expression of any of the four newly identified genes, both 10-deacetylbaccatin III (7) and baccatin III (8) were not produced, thus confirming that each gene is necessary for baccatin III (8) biosynthesis (Figure 4B). Moreover, when leaves were fed a purified epo-taxadiene mix, baccatin III could also be generated by this minimal pathway without TXS (Supplemental Figure 30).

Identification of enzymes catalyzing the last steps of paclitaxel biosynthesis

In the final steps of paclitaxel biosynthesis, the most pressing challenges are to elucidate the reactions leading to the side-chain attachment of β-phenylalanoyl-CoA (11) to baccatin III (8) and its downstream modifications (Figure 5A). This part of the pathway is known to include (i) the conversion of α-phenylalanine to β-phenylalanine (9) by phenylalanine aminomutase (Walker et al., 2004); (ii) the activation of β-phenylalanine to a CoA ester by a β-PCL; (iii) the binding of the side chain by the enzyme baccatin III-3-amino, 13-phenylpropanoyltransferase (BAPT) (Walker et al., 2002a); (iv) the hydroxylation of the side chain at carbon 2′ by an as yet uncharacterized taxane 2′α-hydroxylase (T2′αOH) (Sanchez-Muñoz et al., 2020); and (v) the benzoylation of the product of this reaction by 3′-*N*-debenzoyl-2′-deoxytaxol-*N*-benzoyltransferase (Walker et al., 2002b). An in-depth computational and experimental analysis of a previously analyzed cDNA-amplified fragment length polymorphism (AFLP)c dataset (Ramírez-Estrada et al., 2016) was recently conducted, leading to the identification of transcript TB506 (CYP73A171) as a putative T2′αOH (Sanchez-Muñoz et al., 2020). Molecular docking was conducted to confirm the binding of such a large substrate as 3′N-dehydroxydebenzoyltaxol, with possible docking sites being recognized. Here, we identified that this T2′αOH was subcellularly localized to the ER membrane. Intriguingly, although T2′αOH activity was confirmed in *Pisum sativum* protoplasts, T2′αOHs have not yet been employed in metabolic engineering strategies. Here, we overexpressed *Arabidopsis* benzoate-CoA ligase (BZO) and *Taxus* BAPT, 3′-*N*-debenzoyl-2′-deoxytaxol-*N*-benzoyltransferase, and T2′αOH in

N. benthamiana leaves and co-infiltrated them with benzoic acid, β-phenylalanine-CoA (11), and baccatin III (8). Following co-infiltration, low levels of paclitaxel (14) accumulated in the *N. benthamiana* leaves (Figure 5B; Supplemental Figure 31). The identity of paclitaxel (14) was confirmed by comparison of mass spectra to those of an authentic standard.

Given that one *Penicilium chrysogenum* enzyme (Pc21g30650) has been characterized as β-PCL (Koetsier et al., 2011), we used this gene to replace the *Taxus* homologs that could produce paclitaxel (14) (Figure 5B). Blasting the protein sequence of Pc21g30650 against the *Taxus* genome, we identified seven acyl-activating enzymes (AAEs), including three AAEs from the transcriptomics dataset of the three *Taxus* species (Zhou et al., 2019) (Supplemental Table 1). Given that the products of most paclitaxel biosynthesis genes are subcellularly localized at the ER membrane, it seems likely that the active PCL will also be found at this location (Supplemental Figure 31). Indeed, our experiments confirmed that, similar to the T5αOH and taxadiene-5α-ol-O-acetyl transferase enzymes, this enzyme was localized to the ER membrane (Supplemental Figure 32).

To identify the native *Taxus* β-phenylalanine-CoA ligase, seven co-expressed AAEs were expressed with the suite of enzymes described above (Figure 5A); following feeding with benzoic acid, L-phenylalanine, and baccatin III, we detected a low level of paclitaxel accumulation in the leaves of *N. benthamiana* only upon overexpression of TAAE16 (Figure 5B; Supplemental Figure 31). Thus, after the identification of this PCL and of the T2′αOH, alongside the elucidation of the missing steps in baccatin III biosynthesis, a complete "minimal" pathway for the biosynthesis of paclitaxel could be formulated (Figure 1). Although yields were too low to successfully reconstitute the entire paclitaxel pathway in a single module, the combined analysis that we present suggests not only that the pathway is complete but also that paclitaxel production via synthetic biology approaches is possible.

DISCUSSION

Despite the enormous chemical diversity (close to 600 reported taxane structures and 21 000 recorded chemicals), only the three taxanes paclitaxel, docetaxel, and cabazitaxel have been developed as drugs for the treatment of various types of cancer (Lange and Conner, 2021). The bioactivities of most other taxanes have not been well characterized because of their low levels. Identification of the full paclitaxel biosynthesis pathway should allow us to overcome this limitation by enabling us to purify large quantities of the various taxanes for use in preclinical and clinical trials. Since the release of the sequenced genomes of *Taxus* (Cheng et al., 2021; Xiong et al., 2021; Zhang et al., 2021), many taxane P450s and acetyltransferases have been suggested to be related to taxane biosynthesis. The application of the strategies we presented here will facilitate future research efforts to characterize the biosynthesis of additional useful taxanes.

Although the full pathway was identified, the order of some of the catalytic steps in the pathway remains to be deciphered. Given the very low abundance of the intermediates, the classical approach of ordering the sequence of reactions through isotope tracer experiments does not seem to be feasible. Furthermore, since all these enzymes are subcellularly localized to the ER membrane, and

given that few intermediates can be detected, it is possible that substrate channeling may mediate these reactions (Pareek et al., 2021; Zhang and Fernie, 2021). Future investigations are still needed to identify possible enzyme–enzyme assemblies and substrate channeling. Such studies may also provide insight into the order of the reactions underlying baccatin III (8) biosynthesis.

The metabolic engineering of paclitaxel remains limited to the use of a transient expression system in *N. benthamiana*. Given the low enzyme activities of DBAT, PCL, and BAPT and the toxicity of paclitaxel, both 10-deacetylbaccatin III (7) and baccatin III (8) accumulate to levels 10–20 times greater than paclitaxel in *Taxus* (McElroy and Jennewein, 2018). Moreover, the expression of a mutant *P. chrysogenum* PCL could significantly increase catalytic efficiency (Koetsier et al., 2011). Since we have identified the full pathway, future engineering work on BAPT and PCL will likely greatly improve the efficiency of paclitaxel biosynthesis in stably transformed plants.

Through our combined use of metabolomic analyses and heterologous expression in *N. benthamiana*, we have been able to rapidly establish a complete overview of the complex biosynthetic pathway of paclitaxel, a plant-derived drug of historical and contemporary importance. By combining biosynthetic genes from the medicinal plant *Taxus* with enzymes co-opted from other pathways, we demonstrate *de novo* biosynthetic production of both 10-deacetylbaccatin III (7) and baccatin III (8) in this commonly used model plant. However, given that *N. benthamiana* has diterpenoid-biosynthesis-related genes, we cannot exclude the possibility that the biosynthesis of baccatin III might be assisted by some chaperone proteins, enzymes, or co-factors. Ultimately, our results not only provide a metabolic route to the production of paclitaxel but also highlight a powerful strategy for accelerating the discovery and engineering of natural product biosynthesis in medicinal plants.

METHODS

Chemicals and reagents

Unless stated otherwise, general chemicals and reagents, including 10-deacetylbaccatin III (Sigma, D3676); baccatin III (Sigma, B8154); paclitaxel (Sigma, T7402); L-phenylalanine (Sigma, P2126); DL-β-phenylalanine (Sigma, 159 492); β-phenylalanoyl-CoA (TransMIT, no. P038); taxusin (P) (LGC, CDX-00020082-010); 1-hydroxybaccatin I (TMO-TN2540, TargetMol); 9-dihydro-13-acetylbaccatin III (TMO-T5132, TargetMol); and benzoic acid (Sigma, 242 381), were purchased commercially.

Plant growth

N. benthamiana plants were maintained on growth shelves at the Max Planck Institute of Molecular Plant Physiology with a 16 h light and 8 h dark cycle at 22°C. Plants were grown for 4–5 weeks before *Agrobacterium* infiltration, with periodic watering as needed. *T. baccata* and *T. cuspidata* plant materials were provided by the Botanical Garden of the University of Potsdam. Needles of *T. baccata* and *T. cuspidata* were immediately snap frozen in liquid nitrogen after removal from the plant and stored at −80°C until further use.

Transcriptomic analysis

Additional candidate biosynthetic genes involved in the biosynthesis of paclitaxel were obtained from four published *Taxus* plant RNA-seq datasets (methyl jasmonate-induced *Taxus* cell lines [Ramírez-Estrada et al., 2016; Xiong et al., 2021], three tissues [Kuang et al., 2019], three species [Zhou et al., 2019], and a 10-year-old culture compared with a new culture [Liao

et al., 2017]) using the 13 already characterized paclitaxel biosynthesis genes as bait. The top correlated genes were selected from the different datasets and used for overlap heatmap analysis. The similarly changed genes were selected from different databases prior to this overlap analysis. We only selected candidates that were putatively annotated as having the function of P450s, characterized hydroxylases, PCLs, Pc21g30650, taxane 9α-dioxygenases, or C4β-C20 epoxidases by comparing the sequence homology of similar functional proteins.

cDNA cloning and vector construction

cDNA of the *T. baccata* needles was generated according to a previous publication (Ramírez-Estrada et al., 2016). The 41 paclitaxel biosynthesis genes (Supplemental Table 1) alongside the *Taxus* cytochrome P450 reductase (CPR) were cloned from the cDNA of *T. baccata* by PCR-based Gateway BP cloning using the pDONR207 donor vector (Thermo Fisher Scientific, Waltham, MA, USA). Similarly, ATHMGR and ATBZO were cloned from *Arabidopsis* cDNA. The P19 protein was cloned from pBIN61-P19. Pc21g3065 was cloned from *P. chrysogenum* (Koetsier et al., 2011). The gene-specific primers used did not include a stop codon to ensure C-terminal fusion of tags according to our previous protocol (Zhang et al., 2019) (Supplemental Table 2). For subcellular localization, all genes were subcloned into PK7FWG2 with a C-terminal GFP tag. The pBin-ER-mCherry was used as the subcellular localization marker (Nelson et al., 2007). All the paclitaxel biosynthesis genes were subsequently cloned under the control of the 35S promoter and terminator using gene-specific primers with stop codons using In-Fusion (Takara Bio) technology, while both CPR and AtBZO were linked with the CsMV promoter and terminator of Arabidopsis actin 8 (Supplemental Table 4). All four genes were linked by two-step In-Fusion (Takara Bio) using two pairs of promoter- and terminator-specific primers (Supplemental Table 2). Finally, these genes were subcloned into pK7m34GW2-8m21GW3 or pK7WG2 (VIB) using the LR reaction-based construction of expression vectors. The vectors constructed in this study are listed in Supplemental Table 3.

Agroinfiltration

Frozen stocks of AGL1 *Agrobacterium* electrocompetent cells were added to YEB medium with Carb25 mg/l carbenicillin) and Rif (20 mg/l rifampicin) and incubated at 28°C overnight. The cells were centrifuged for 30 s at 20 000 *g* at 4°C and washed with 1 ml and 500 μl ice-cold water. The cells were finally resuspended in 200 μl water (these cells are subsequently referred to as *Agrobacteria* competent cells). Around 100 ng expression plasmid was added into a 2 ml tube with 45 μl *Agrobacteria* competent cells on ice for 5 min. The solution was electrically shocked in cuvettes and maintained at 28°C with 1 ml YEB medium. After shaking for 1–2 h at 28°C at 250 rpm, the cells were plated on a YEB plate (containing Carb, Rif, and appropriate antibiotics) and incubated at 28°C for 2–3 days.

The *Agrobacteria* were grown on YEB-induced medium plates at 28°C for 24–36 h (Zhang et al., 2020). The cells were scratched and resuspended in 500 μl washing solution (10 mM MgCl₂, 100 μM acetosyringone). After a short vortex, the 100 μl resuspended *Agrobacteria* were diluted 10 times and the OD₆₀₀ was measured (should be equal to or greater than 12). The *Agrobacteria* were finally diluted to OD₆₀₀ = 1 in infiltration solution (¼ Murashige and Skoog [pH = 6.0], 1% sucrose, 100 μM acetosyringone, 0.005% [v/v, 50 μl/l] Silwet L-77). The *Agrobacteria* were infiltrated into *N. benthamiana* leaves using a 1 ml plastic syringe. The plants were kept in the light to dry the leaves (1 h), and then subsequently kept in the dark for 3–4 days at room temperature. Unless stated otherwise, each experimental condition tested consisted of at least two replicates, with each replicate corresponding to an independently infiltrated leaf. Each leaf among these two replicates was selected from a different *N. benthamiana* plant such that no replicates for one experimental condition were taken from the same plant. In general, infiltrated leaves were harvested 4–5 days after infiltration, snap frozen in liquid nitrogen, and stored at −80°C for downstream processing.

Confocal analysis

Constructs were transiently expressed in *N. benthamiana* leaves by agro-infiltration as described above for the protein co-sublocalization analysis. Confocal images were taken using a DM6000B/SP8 confocal laser scanning microscope.

GC–MS

For GC–MS analysis of taxa-4(5),11(12)-diene, iso-OCT, OCT, and taxadiene-5α-ol, plant materials (needles from *T. baccata*) were collected and ground to a powder in liquid nitrogen. According to a previously published protocol (Li et al., 2019), around 1 g plant material was extracted three times by 1 ml hexane with 20 min of shaking and 20 min of sonication. Samples were then extracted once with a hexane:ethyl acetate mixture (4:1 v/v). The organic solvent phases were combined and dried under a stream of nitrogen. The sample (1 μl) was injected into the GC–MS in splitless mode in a Thermo Scientific TRACE 1300 Series Gas Chromatograph by ZB-5 column (Phenomenex). The retention times of taxa-4(5),11(12)-diene (*m/z* 272), OCT (*m/z* 288), and taxadiene-5α-ol (*m/z* 288) were comparable with those from the yeast extraction positive control, and the products were further confirmed by NMR (Supplemental Table 4) (Walls et al., 2022).

For GC–MS profiling analysis of other intermediates from 4β,20-taxadiene and 4β,20-taxadiene-5α-ol, plant material was collected and ground to a powder in liquid nitrogen. Around 1 g plant material was extracted by 650 μl ethyl acetate with 30 min of shaking and 10 min of sonication. After centrifuging at 16 000 *g* for 5 min, the 600 μl supernatant was transferred to a fresh 2 ml tube. Subsequently, 500 μl ethyl acetate was added, and the sample was vortexed and sonicated twice. After repeating this step and collecting all the ethyl acetate extract (around 1600 μl), the supernatants were dried under a stream of nitrogen gas. Given that a high concentration of chlorophyll results in low-quality GC–MS profiles, the dried extracts were treated with 100% methanol for 10 min of vortexing and 10 min of sonication at 4°C. After adding 200 μl CHCl₃, 600 μl ddH₂O was added to extract the polar metabolites. The supernatant was subsequently dried under a stream of gas. Trimethylsilylation was performed by adding a 50 μl mixture of *N,O*-bis(trimethylsilyl)trifluoroacetamide and an *n*-alkane standard mix in hexane (7:1, v/v), followed by incubation at 37°C for 30 min with gentle shaking (800 rpm). The sample (1 μl) was injected into the GC–MS in splitless mode.

Metabolite profiling was performed as detailed previously by GC coupled to electron impact ionization/time-of-flight MS using an Agilent 6890N24 gas chromatograph (Agilent Technologies) connected to a Pegasus III time-of-flight mass spectrometer (LECO Instrumente, Mönchengladbach, Germany) (Erban et al., 2007). Data analysis was performed with Xcalibur software (Thermo Fisher Scientific). The retention times of 4β,20-taxadiene (*m/z* 288, room temperature, 21.70) and 4β,20-taxadiene-5α-triol (*m/z* 376, 1TMS room temperature, 22.33) were determined by comparing peaks of the expected masses in the samples and controls (Supplemental Table 4).

Ultra-high-performance LC HRMS (UHPLC–HRMS)

For UHPLC–HRMS profiling analysis, plant material was collected and ground to a powder in liquid nitrogen. Around 50 mg plant material was extracted using the methyl-*tert*-butyl-ether:methanol (MeOH) extraction method (Salem et al., 2020). Both the upper and lower phases were dried in a vacuum concentrator before being resuspended in 200 μl acetonitrile:isopropanol (70:30, upper phase) or 50% methanol (lower phase) and transferred to a glass vial for UHPLC–HRMS metabolomic profiling. The UHPLC–HRMS system consisted of a Waters Acquity UPLC coupled to an Exactive Orbitrap mass detector according to a previously published protocol (Alseekh et al., 2015; Perez de Souza et al., 2019). The UPLC system was equipped with an HSS T3 C₁₈ reversed-phase column (100 × 2.1 mm i.d., 1.8 μm particle size; Waters) that was operated at a temperature of 40°C. The mobile phases consisted of 0.1% formic acid in water (solvent A) and 0.1% formic acid in acetonitrile (solvent B). The flow rate of

the mobile phase was 400 μl/min, and 2 μl sample was injected. The UPLC was connected to an Exactive Orbitrap (Thermo Fisher Scientific) via a heated electrospray source (Thermo Fisher Scientific). The spectra were recorded using the full scan mode of positive ion detection modes, covering a mass range from m/z 100 to 1500. The resolution was set to 25 000, and the maximum scan time was set to 250 ms. The sheath gas was set to a value of 60, while the auxiliary gas was set to 35. The transfer capillary temperature was set to 150°C, while the heater temperature was adjusted to 300°C. The spray voltage was fixed at 3 kV, with a capillary voltage and a skimmer voltage of 25 and 15 V, respectively. MS spectra were recorded from min 0 to 19 of the UPLC gradient. Molecular masses, retention time, and associated peak intensities were extracted from the raw files using Xcalibur software (Thermo Fisher Scientific). Metabolite identification and annotation were performed using standard compounds and the monoisotopic mass of predicted compounds. Data are reported in Supplemental Table 5 in a manner compliant with the literature standards (Alseekh et al., 2021; Perez de Souza et al., 2021).

NMR spectroscopy

^{1}H NMR spectral data were recorded on a BRUKER (AVANCE III 700) spectrometer in the reported deuterated solvents. The chemical shifts (δ) are listed in parts per million (ppm) and are reported relative to the corresponding residual nondeuterated solvent signal (CDCl$_3$: δ$_H$ = 7.26 ppm, δ$_C$ = 77.2 ppm). Integrals are in accordance with assignments, and coupling constants (J) are given in Hz. Multiplicity is indicated as follows: s (singlet), d (doublet), t (triplet), br (broad), and combinations thereof. When no multiplicity could be identified, the chemical shift range of the signal is given as m (multiplet).

Chemical reaction experiments

Taxadiene (1 mg, 0.0036 mM) was mixed with CH$_2$Cl$_2$ (1 ml) and NaHCO$_3$ (0.5 mg, 0.05 mmol) in a 14 ml Pyrex glass tube. mCPBA (20 μl 25 mM stock, calculated assuming a nominal purity of 70%) was added, and the reaction proceeded for 2 h. The crude product mixture was subsequently washed twice with saturated sodium carbonate and once with NaS$_2$O$_3$. The organic layer was transferred and dried for GC–MS analysis. Similarly, the DMDO reaction was performed by adding 0.34 mg taxadiene (0.00125 mM) to 250 μl EA and 250 μl water (buffered with 0.66 mg sodium carbonate) with 10 μl acetate. Oxone in water (4.8 mg in 1 ml) and a solution of acetone and sodium carbonate in water (18 μl and 0.66 mg, respectively, in 1 ml) were added dropwise as separate solutions over a period of 2 h. Sodium carbonate was used as final buffering reagent after quenching the reaction. The reaction mixture was analyzed by GC–MS.

The deacetylation of taxusin, 1-hydroxybaccatin I, and 9-dihydro-13-acetylbaccatin III was performed by global reductive removal of the acetates with LiAlH$_4$ as described by previous research (Li et al., 2008), and the reaction products were confirmed by UHPLC–HRMS. Taxusin-4β,20-epoxide was synthesized from taxusin by peracetic acid as described in previous research (Kaspera et al., 2010), separately by normal-phase HPLC, confirmed by NMR. The produce was subsequently measured using an acquit UPLC system equipped with an RP C8 column and analyzed by MS as standard (Salem et al., 2020).

13-Acetyl baccatin III was synthesized via a reaction similar to the synthesis of 13-butyrylbaccatin III (Ondari and Walker, 2008) as previously described and was subsequently confirmed by NMR and LC–MS. Both taxadiene-5α-ol and taxadiene-5α-acetyl were additionally synthetized as previously described and confirmed by NMR and GC–MS (Kanda et al., 2020).

In addition, epoxidase was linked into p5T7tds-ggpps and co-transformed with pSEVA228-pro4IUPi (Chatzivasileiou et al., 2019) into *E. coli*. After 24 h of incubation with prenol, isopernol, and IPTG, only taxadiene could be detected. The epoxidase was also subcloned into pYES-DEST52 and transformed into LRS5 (Nowrouzi et al., 2020), which could produce taxadiene. However, after galactose inducible, only taxadiene could be detected.

Enzyme assay

The epoxidase was transiently expressed in *N. benthamiana* leaves by agroinfiltration. A leaf disc was fed taxusin in $\frac{1}{4}$ Murashige and Skoog medium for a 12 h reaction period. Metabolism was quenched with liquid nitrogen, and samples were extracted using the methyl-*tert-butyl-ether* method and measured by an Acquity UPLC system using an RP C8 column and analyzed by MS (Salem et al., 2020).

SUPPLEMENTAL INFORMATION

Supplemental information is available at *Molecular Plant Online*.

AUTHOR CONTRIBUTIONS

Y.Z. conceived the project and experiments. A.R.F. acquired the funding. A.R.F. supervised the project. Y.Z. analyzed transcriptomic data, characterized biosynthetic genes, and established the metabolic engineering strategy. L.W., H.F., J.J.M., and M.C. helped the with the chemical synthesis and NMR measurement. S.A, . performed LC-–MS measurements. L.P.d.S. and F.S. checked all chromatography data. L.W., H.F., J.J.M., and M.C. performed chemical synthesis. Y.Z. and A.R.F. wrote the manuscript. Y.Z., L.P.d.S., F.S., and A.R.F. revised the manuscript.

ACKNOWLEDGMENTS

REFERENCES

Ajikumar, P.K., Xiao, W.-H, Tyo, K.E.J., Wang, Y., Simeon, F., Leonard, E., Mucha, O., Phon, T.H., Pfeifer, B., and Stephanopoulos, G. (2010). Isoprenoid pathway optimization for Taxol precursor overproduction in Escherichia coli. Science **330**:70–74.

Alseekh, S., Aharoni, A., Brotman, Y., Contrepois, K., D'Auria, J., Ewald, J., C Ewald, J., Fraser, P.D., Giavalisco, P., Hall, R.D., et al. (2021). Mass spectrometry-based metabolomics: A guide for annotation, quantification and best reporting practices. Nat. Methods **18**:747–756.

Alseekh, S., Tohge, T., Wendenberg, R., Scossa, F., Omranian, N., Li, J., Kleessen, S., Giavalisco, P., Pleban, T., Mueller-Roeber, B., et al. (2015). Identification and mode of inheritance of quantitative trait loci for secondary metabolite abundance in tomato. Plant Cell **27**:485–512.

Chatzivasileiou, A.O., Ward, V., Edgar, S.M., and Stephanopoulos, G. (2019). Two-step pathway for isoprenoid synthesis. Proc. Natl. Acad. Sci. USA **116**:506–511.

Chau, M., Jennewein, S., Walker, K., and Croteau, R. (2004a). Taxol biosynthesis: molecular cloning and characterization of a cytochrome P450 taxoid 7β-hydroxylase. Chem. Biol. **11**:663–672.

Chau, M., Walker, K., Long, R., and Croteau, R. (2004b). Regioselectivity of taxoid-O-acetyltransferases: heterologous expression and characterization of a new taxadien-5α-ol-O-acetyltransferase. Arch. Biochem. Biophys. **430**:237–246.

Cheng, J., Wang, X., Liu, X., Zhu, X., Li, Z., Chu, H., Wang, Q., Lou, Q., Cai, B., Yang, Y., et al. (2021). Chromosome-level genome of Himalayan yew provides insights into the origin and evolution of the paclitaxel biosynthetic pathway. Mol. Plant **14**:1199–1209.

De La Peña, R., and Sattely, E.S. (2021). Rerouting plant terpene biosynthesis enables momilactone pathway elucidation. Nat. Chem. Biol. **17**:205–212.

Edgar, S., Li, F.-S., Qiao, K., Weng, J.-K., and Stephanopoulos, G. (2017). Engineering of taxadiene synthase for improved selectivity and yield of a key taxol biosynthetic intermediate. ACS Synth. Biol. **6**:201–205.

Erban, A., Schauer, N., Fernie, A.R., and Kopka, J. (2007). Nonsupervised construction and application of mass spectral and retention time index libraries from time-of-flight gas chromatography-mass spectrometry metabolite profiles. In Metabolomics (Springer), pp. 19–38.

Fischer, J., and Ganellin, C.R. (2010). Analogue-based drug discovery. Chemistry International–Newsmagazine for IUPAC **32**:12–15.

Guerra-Bubb, J., Croteau, R., and Williams, R.M. (2012). The early stages of taxol biosynthesis: an interim report on the synthesis and identification of early pathway metabolites. Nat. Prod. Rep. **29**:683–696.

Jennewein, S., Rithner, C.D., Williams, R.M., and Croteau, R.B. (2001). Taxol biosynthesis: taxane 13α-hydroxylase is a cytochrome P450-dependent monooxygenase. Proc. Natl. Acad. Sci. USA **98**:13595–13600.

Kanda, Y., Ishihara, Y., Wilde, N.C., and Baran, P.S. (2020). Two-phase total synthesis of taxanes: tactics and strategies. J. Org. Chem. **85**:10293–10320.

Kaspera, R., Cape, J.L., Faraldos, J.A., Ketchum, R.E.B., and Croteau, R.B. (2010). Synthesis and in vitro evaluation of taxol oxetane ring D precursors. Tetrahedron Lett. **51**:2017–2019.

Koetsier, M.J., Jekel, P.A., Wijma, H.J., Bovenberg, R.A.L., and Janssen, D.B. (2011). Aminoacyl-coenzyme A synthesis catalyzed by a CoA ligase from Penicillium chrysogenum. FEBS Lett. **585**:893–898.

Köksal, M., Jin, Y., Coates, R.M., Croteau, R., and Christianson, D.W. (2011). Taxadiene synthase structure and evolution of modular architecture in terpene biosynthesis. Nature **469**:116–120.

Kuang, X., Sun, S., Wei, J., Li, Y., and Sun, C. (2019). Iso-Seq analysis of the Taxus cuspidata transcriptome reveals the complexity of Taxol biosynthesis. BMC Plant Biol. **19**:210–216.

Lange, B.M., and Conner, C.F. (2021). Taxanes and taxoids of the genus Taxus–A comprehensive inventory of chemical diversity. Phytochemistry **190**, 112829.

Li, H., Horiguchi, T., Croteau, R., and Williams, R.M. (2008). Studies on Taxol biosynthesis: preparation of taxadiene-diol and triol derivatives by deoxygenation of taxusin. Tetrahedron **64**:6561–6567.

Li, J., Mutanda, I., Wang, K., Yang, L., Wang, J., and Wang, Y. (2019). Chloroplastic metabolic engineering coupled with isoprenoid pool enhancement for committed taxanes biosynthesis in Nicotiana benthamiana. Nat. Commun. **10**:4850–4912.

Liao, W., Zhao, S., Zhang, M., Dong, K., Chen, Y., Fu, C., and Yu, L. (2017). Transcriptome assembly and systematic identification of novel cytochrome P450s in Taxus chinensis. Front. Plant Sci. **8**:1468.

Lucas, H. (1856). Ueber ein in den Blättern von Taxus baccata L. enthaltenes Alkaloid (das Taxin). Arch. Pharmazie **135**:145–149.

McElroy, C., and Jennewein, S. (2018). Taxol® biosynthesis and production: from forests to fermenters. In Biotechnology of Natural Products (Springer), pp. 145–185.

Mutanda, I., Li, J., Xu, F., and Wang, Y. (2021). Recent Advances in Metabolic Engineering, Protein Engineering, and Transcriptome-Guided Insights Toward Synthetic Production of Taxol. Front. Bioeng. Biotechnol. **9**:632269.

Mutwil, M. (2020). Computational approaches to unravel the pathways and evolution of specialized metabolism. Curr. Opin. Plant Biol. **55**:38–46.

Nazhand, A., Durazzo, A., Lucarini, M., Mobilia, M.A., Omri, B., and Santini, A. (2020). Rewiring cellular metabolism for heterologous biosynthesis of Taxol. Nat. Prod. Res. **34**:110–121.

Nelson, B.K., Cai, X., and Nebenführ, A. (2007). A multicolored set of in vivo organelle markers for co-localization studies in Arabidopsis and other plants. Plant J. **51**:1126–1136.

Nicolaou, K., Yang, Z., Liu, J.J., Ueno, H., Nantermet, P., Guy, R., Claiborne, C., Renaud, J., Couladouros, E., and Paulvannan, K. (1994). Total synthesis of taxol. Nature **367**:630–634.

Nowrouzi, B., Li, R.A., Walls, L.E., d'Espaux, L., Malcı, K., Liang, L., Jonguitud-Borrego, N., Lerma-Escalera, A.I., Morones-Ramirez, J.R., Keasling, J.D., et al. (2020). Enhanced production of taxadiene in Saccharomyces cerevisiae. Microb. Cell Factories **19**:200–212.

Ondari, M.E., and Walker, K.D. (2008). The taxol pathway 10-O-acetyltransferase shows regioselective promiscuity with the oxetane hydroxyl of 4-deacetyltaxanes. J. Am. Chem. Soc. **130**:17187–17194.

Onrubia, M., Moyano, E., Bonfill, M., Cusidó, R.M., Goossens, A., and Palazón, J. (2013). Coronatine, a more powerful elicitor for inducing taxane biosynthesis in Taxus media cell cultures than methyl jasmonate. J. Plant Physiol. **170**:211–219.

Onrubia, M., Pollier, J., Vanden Bossche, R., Goethals, M., Gevaert, K., Moyano, E., Vidal-Limon, H., Cusidó, R.M., Palazón, J., and Goossens, A. (2014). Taximin, a conserved plant-specific peptide is involved in the modulation of plant-specialized metabolism. Plant Biotechnol. J. **12**:971–983.

Pareek, V., Sha, Z., He, J., Wingreen, N.S., and Benkovic, S.J. (2021). Metabolic channeling: predictions, deductions, and evidence. Mol. Cell **81**:3775–3785.

Perez de Souza, L., Alseekh, S., Naake, T., and Fernie, A. (2019). Mass spectrometry-based untargeted plant metabolomics. Curr. Protoc. Plant Biol. **4**, e20100.

Perez de Souza, L., Alseekh, S., Scossa, F., and Fernie, A.R. (2021). Ultra-high-performance liquid chromatography high-resolution mass spectrometry variants for metabolomics research. Nat. Methods **18**:733–746.

Ramírez-Estrada, K., Altabella, T., Onrubia, M., Moyano, E., Notredame, C., Osuna, L., Vanden Bossche, R., Goossens, A., Cusido, R.M., and Palazon, J. (2016). Transcript profiling of jasmonate-elicited Taxus cells reveals a β-phenylalanine-CoA ligase. Plant Biotechnol. J. **14**:85–96.

Roberts, S.C. (2007). Production and engineering of terpenoids in plant cell culture. Nat. Chem. Biol. **3**:387–395.

Rontein, D., Onillon, S., Herbette, G., Lesot, A., Werck-Reichhart, D., Sallaud, C., and Tissier, A. (2008). CYP725A4 from yew catalyzes complex structural rearrangement of taxa-4 (5), 11 (12)-diene into the cyclic ether 5 (12)-oxa-3 (11)-cyclotaxane. J. Biol. Chem. **283**:6067–6075.

Salem, M.A., Yoshida, T., Perez de Souza, L., Alseekh, S., Bajdzienko, K., Fernie, A.R., and Giavalisco, P. (2020). An improved extraction method enables the comprehensive analysis of lipids, proteins, metabolites and phytohormones from a single sample of leaf tissue under water-deficit stress. Plant J. **103**:1614–1632.

Sanchez-Muñoz, R., Perez-Mata, E., Almagro, L., Cusido, R.M., Bonfill, M., Palazon, J., and Moyano, E. (2020). A novel hydroxylation step in the taxane biosynthetic pathway: a new approach to paclitaxel production by synthetic biology. Front. Bioeng. Biotechnol. **8**:410.

Walker, K., Fujisaki, S., Long, R., and Croteau, R. (2002a). Molecular cloning and heterologous expression of the C-13 phenylpropanoid side chain-CoA acyltransferase that functions in Taxol biosynthesis. Proc. Natl. Acad. Sci. USA **99**:12715–12720.

Walker, K., Long, R., and Croteau, R. (2002b). The final acylation step in taxol biosynthesis: cloning of the taxoid C13-side-chain N-benzoyltransferase from Taxus. Proc. Natl. Acad. Sci. USA **99**:9166–9171.

Walker, K.D., Klettke, K., Akiyama, T., and Croteau, R. (2004). Cloning, heterologous expression, and characterization of a phenylalanine aminomutase involved in Taxol biosynthesis. J. Biol. Chem. **279**:53947–53954.

Walls, L.E., Martinez, J.L., and Rios-Solis, L. (2022). Enhancing Saccharomyces cerevisiae taxane biosynthesis and overcoming nutritional stress-induced pseudohyphal growth. Microorganisms **10**:163.

Wani, M.C., Taylor, H.L., Wall, M.E., Coggon, P., and McPhail, A.T. (1971). Plant antitumor agents. VI. Isolation and structure of taxol, a novel antileukemic and antitumor agent from Taxus brevifolia. J. Am. Chem. Soc. **93**:2325–2327.

Xiong, X., Gou, J., Liao, Q., Li, Y., Zhou, Q., Bi, G., Li, C., Du, R., Wang, X., Sun, T., et al. (2021). The Taxus genome provides insights into paclitaxel biosynthesis. Nat. Plants **7**:1026–1036.

Yang, C.-P.H., and Horwitz, S.B. (2017). Taxol®: the first microtubule stabilizing agent. Int. J. Mol. Sci. **18**:1733.

You, L.-F., Huang, J.-J., Wei, T., Lin, S.-L., Jiang, B.-H., Guo, L.-Q., and Lin, J.-F. (2018). Enhanced catalytic activities and modified substrate preferences for taxoid 10β-O-acetyl transferase mutants by engineering catalytic histidine residues. Biotechnol. Lett. **40**:1245–1251.

Zhang, Y., Chen, M., Siemiatkowska, B., Toleco, M.R., Jing, Y., Strotmann, V., Zhang, J., Stahl, Y., and Fernie, A.R. (2020). A highly efficient agrobacterium-mediated method for transient gene expression and functional studies in multiple plant species. Plant Commun. **1**, 100028.

Zhang, Y., and Fernie, A.R. (2021). Metabolons, enzyme–enzyme assemblies that mediate substrate channeling, and their roles in plant metabolism. Plant Commun. **2**, 100081.

Zhang, Y., Natale, R., Domingues, A.P., Toleco, M.R., Siemiatkowska, B., Fàbregas, N., and Fernie, A.R. (2019). Rapid identification of protein-protein interactions in plants. Curr. Protoc. Plant Biol. **4**, e20099.

Zhang, Y., Scossa, F., and Fernie, A.R. (2021). The genomes of Taxus species unveil novel candidates in the biosynthesis of taxoids. Mol. Plant **14**:1773–1775.

Zhou, K., Qiao, K., Edgar, S., and Stephanopoulos, G. (2015). Distributing a metabolic pathway among a microbial consortium enhances production of natural products. Nat. Biotechnol. **33**:377–383.

Zhou, T., Luo, X., Yu, C., Zhang, C., Zhang, L., Song, Y.-b., Dong, M., and Shen, C. (2019). Transcriptome analyses provide insights into the expression pattern and sequence similarity of several taxol biosynthesis-related genes in three Taxus species. BMC Plant Biol. **19**:33.